



Assessment and quantification of NO_x sources at a regional background site in North China: Comparative results from a Bayesian isotopic mixing model and a positive matrix factorization model

Zheng Zong^{a, b}, Yang Tan^a, Xiaoping Wang^b, Chongguo Tian^{a, *}, Yunting Fang^c, Yingjun Chen^d, Yin Fang^d, Guangxuan Han^a, Jun Li^b, Gan Zhang^b

^a Key Laboratory of Coastal Environmental Processes and Ecological Remediation, Yantai Institute of Coastal Zone Research, Chinese Academy of Sciences, Yantai, 264003, China

^b State Key Laboratory of Organic Geochemistry, Guangzhou Institute of Geochemistry, Chinese Academy of Sciences, Guangzhou, 510640, China

^c Key Laboratory of Forest Ecology and Management, Institute of Applied Ecology, Chinese Academy of Sciences, Shenyang, Liaoning, 110164, China

^d Key Laboratory of Cities' Mitigation and Adaptation to Climate Change in Shanghai (CMA), College of Environmental Science and Engineering, Tongji University, Shanghai, 200092, China

ARTICLE INFO

Article history:

Received 9 March 2018

Received in revised form

13 July 2018

Accepted 8 August 2018

Available online 14 August 2018

Keywords:

NO_x sources

Nitrogen/oxygen isotope

Bayesian isotopic mixing model

PMF model

ABSTRACT

Regional sources of nitrogen oxides (NO_x) in North China during summer were explored using both a Bayesian isotopic mixing model and a positive matrix factorization (PMF) model. Results showed that the nitrogen isotope ($\delta^{15}\text{N}$) composition of particulate nitrate (NO_3^-) varied between -8.9‰ and $+14.1\text{‰}$, while the oxygen isotope ($\delta^{18}\text{O}$) composition ranged from $+57.4\text{‰}$ to $+93.8\text{‰}$. Based on results from the Bayesian isotopic mixing model, the contribution of the hydroxyl radical ($\bullet\text{OH}$) NO_x conversion pathway showed clear diurnal fluctuation; values were higher during the day (0.53 ± 0.16) and lower overnight (0.42 ± 0.17). Values peaked at 06:00–12:00 and then decreased gradually until 00:00–06:00 the next day. Coal combustion ($31.34 \pm 9.04\%$) was the most significant source of NO_x followed by biomass burning ($25.74 \pm 2.58\%$), mobile sources ($23.83 \pm 3.66\%$), and microbial processes ($19.09 \pm 5.21\%$). PMF results indicated that the contribution from mobile sources was 19.83%, slightly lower as compared to the Bayesian model (23.83%). The PMF model also reported a lower contribution from coal combustion (28.65%) as compared to the Bayesian model (31.34%); however, the sum of biomass burning and microbial processes in the Bayesian model (44.83%) was lower than the aggregate of secondary inorganic aerosol, sea salt, and soil dust in PMF model (51.52%). Overall, differences between the two models were minor, suggesting that this study provided a reasonable source quantification for NO_x in North China during summer.

© 2018 Elsevier Ltd. All rights reserved.

1. Introduction

China suffers from severe air pollution, attributed to anthropogenic emissions of reactive gases, of which nitrogen oxides (NO_x) is thought to play a key role (Liu et al., 2013). NO_x regulates atmospheric oxidants (e.g., O₃ and $\bullet\text{OH}$), markedly impacting atmospheric chemistry, and has been found to accelerate the formation of new particles (Cheng et al., 2016; Hastings et al., 2004). This phenomenon may explain why particulate pollution occurs frequently in China, because the emission of NO_x has increased in

accordance with rapid economic development. Total NO_x emissions were approximately 10 million tons in 1995, and reached 24 million tons in 2011, an increase of more than 50% (<http://www.zhb.gov.cn>). In light of this increase, the State Council released the “Twelfth Five-Year Plan for National Environmental Protection”, prescribing control measures for NO_x as one of two new strategies for pollution control. Although NO_x emissions have been declining in recent years, total emissions remain at approximately 20 million tons, which approaches or exceeds the upper limits of the environmental carrying capacity. Consequently, reducing NO_x emissions in China remains an arduous challenge. Accurate information regarding NO_x emission sources are important for their effective control, especially in the heavily polluted region of North China

* Corresponding author.

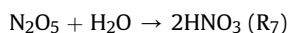
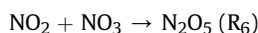
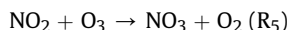
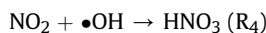
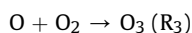
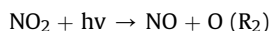
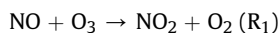
E-mail address: cgtian@yic.ac.cn (C. Tian).

(Yang et al., 2015).

Atmospheric NO_x has both anthropogenic and natural origins, including fossil fuel combustion, biomass burning, and soil emissions (Hastings et al., 2009; Miller et al., 2017). Because of these varied origins, quantifying NO_x sources is difficult. This has encouraged researchers to develop techniques to estimate the individual contribution of NO_x sources. For example, the analysis of stable nitrogen isotopes in particulate nitrate ($\delta^{15}\text{N}-\text{NO}_3^-$) provides a powerful tool to determine NO_x sources due to the fact that N atoms are conserved during the transformation of NO_x into NO_3^- in the atmosphere (Wang et al., 2017b). Under the “1-atm” concept, the sources of derived NO_3^- would be consistent with those of their precursor NO_x . Furthermore, the N isotopic signature of different anthropogenic and natural NO_x sources usually varies over an extensive range (Fibiger and Hastings, 2016). Although the impact of kinetic and equilibrium isotopic fractionation of $\delta^{15}\text{N}$ during the conversion of NO_x to NO_3^- must be considered, previous studies have suggested that $\delta^{15}\text{N}-\text{NO}_3^-$ could be linked to NO_x sources (Elliott et al., 2007; Wankel et al., 2010). However, isotopic technology can only qualitatively identify NO_x sources, and other top-down constraints are necessary to quantify the sources of NO_x . For example, the Bayesian isotopic mixing model can estimate the contribution of different sources in a mixture and is widely applied in ecology (Parnell et al., 2013). After incorporating fractionation when evaluating the isotopic fractionation of the equilibrium/Leighton reaction, the model is more suitable for apportioning NO_x sources, and was first employed in China in our previous study (Zong et al., 2017). Positive matrix factorization (PMF) is another useful receptor model for quantitatively analyzing sources of pollutants. In published works, the model has been used to apportion aggregate pollutants, including fine particles ($\text{PM}_{2.5}$) and polycyclic aromatic hydrocarbons (Bressi et al., 2014; Fang et al., 2016), while also offering source data for individual components including organic carbon (OC) and elemental carbon (EC) (Huang et al., 2014). In this study, PMF is used in conjunction with the Bayesian isotopic mixing model to apportion the sources of NO_3^- in $\text{PM}_{2.5}$, providing more precise data to aid in the control of NO_x pollution.

Once emitted into the atmosphere, NO_x is oxidized to HNO_3 or NO_3^- via the following chemical pathways (R_1-R_8) (Fang et al., 2011). In summary, NO_x oxygen atoms are rapidly exchanged with O_3 in the NO/NO_2 cycle (R_1-R_3); $\bullet\text{OH}$ radicals result in the oxidation of NO_2 to HNO_3 (R_4 ; the $\bullet\text{OH}$ pathway); NO_2 is oxidized by O_3 to produce NO_3 (R_5), which subsequently combines with NO_2 to form N_2O_5 (R_6), and then undergoes hydrolysis to form HNO_3 (R_7), referred to as the O_3 pathway; and the generated HNO_3 combines with alkali to form NO_3^- (R_8). Overall, the $\bullet\text{OH}$ and O_3 pathways are the two fundamental oxidation pathways for NO_x , generally exhibiting noticeable diurnal and seasonal variation. Previous research has found that the $\bullet\text{OH}$ pathway is more prevalent during the daytime and in summer, when the relative concentration of $\bullet\text{OH}$ is higher. Conversely, the O_3 pathway is more dominant overnight and in winter, because N_2O_5 is thermally unstable (Hastings et al., 2003; Xiao et al., 2015). However, quantifying the respective ratios of the two pathways remains a challenge. Furthermore, the impact of environmental factors (e.g., wind speed, temperature, and relative humidity) on NO_x conversion processes is rarely explored; this could provide substantial insight for NO_x induced particle management. In this study, the Yellow River Delta, a regional background site in North China, is chosen to investigate summer NO_x sources. An improved Bayesian model (stable isotope mixing model using sampling-importance-resampling; MixSIR) is utilized to obtain the quantitative source outcome of NO_x , which is then validated by the PMF model. Additionally, the relationship between environmental factors and NO_3^- formation, and the diurnal contribution ratio of the two basic NO_x oxidation pathways is

explored. Based on the N isotopic signature, geographical and diurnal source characteristics of NO_x are also discussed. This investigation will aid in the development of efficient remediation policies to improve the air quality in the severely polluted region of North China.



2. Materials and methods

2.1. Sampling site and sampling procedure

$\text{PM}_{2.5}$ samples were collected using a Tisch high volume sampler at a flow rate of $1.13 \text{ m}^3 \text{ min}^{-1}$ from 29 May to 1 July 2013 at the Yellow River Delta Ecological Research Station of Coastal Wetland ($37^\circ 45' \text{N}$, $118^\circ 59' \text{E}$), Chinese Academy of Sciences (YRD). The station is located approximately 3 km south of the Yellow River channel and approximately 20 km southwest of the river mouth, where no nearby anthropogenic NO_x sources were apparent (Han et al., 2015). With a climate dominated by the East Asian summer monsoon, prevailing winds are predominantly from the Shandong and Jiangsu Provinces (see Fig. S1). Local meteorological parameters (wind speed, temperature, and relative humidity) were obtained using a Three-Dimensional Ultrasonic Anemometer (CSAT-3, Campbell Scientific, Logan, USA) and a weather station (Vantage Pro 2, Davis, USA). Observations were recorded at two sampling intervals (12 and 6 hourly); 12 hourly samples were collected from 06:00–18:00 (daytime) and 18:00–06:00 (night time); 6 hourly samples were collected from 06:00–12:00, 12:00–18:00, 18:00–00:00, and 00:00–06:00. Six hourly sampling was performed from 1 June 18:00 to 6 June 06:00 and from 18 June 18:00 to 21 June 18:00, and 12 hourly sampling was conducted for the remainder of the sampling period. In total, 76 samples were collected throughout the sampling campaign. To minimize experimental error, quartz fiber filters were preheated at 450°C for 6 h in a muffle furnace to remove impurities. After sampling, filters were folded, wrapped in aluminum foil, sealed in airtight plastic bags, and then refrigerated (-20°C) until analysis to prevent evaporation of volatile components.

2.2. Isotope and chemical analysis

The N_2O isotope analysis method was adopted to quantify $\delta^{15}\text{N}$ and stable oxygen isotope ($\delta^{18}\text{O}$) values for NO_3^- in this study (McIlvin and Altabet, 2005). To summarize, NO_3^- from the filter extract was initially reduced to nitrite (NO_2^-) using cadmium powder, and NO_2^- was further reduced to N_2O using sodium azide in an acetic acid buffer. Then, $\delta^{15}\text{N}$ and $\delta^{18}\text{O}$ of the converted N_2O were analyzed using an isotope ratio mass spectrometer (MAT253,

Thermo Fisher Scientific, Waltham, MA, USA). The detected $\delta^{15}\text{N}$ and $\delta^{18}\text{O}$ values were reported in parts per thousand relative to standards (international reference materials: IAEA–NO–3, USGS32, USGS34, and USGS35):

$$\delta^{15}\text{N} = \left[\left(\frac{^{15}\text{N}/^{14}\text{N}}{^{15}\text{N}/^{14}\text{N}} \right)_{\text{sample}} / \left(\frac{^{15}\text{N}/^{14}\text{N}}{^{15}\text{N}/^{14}\text{N}} \right)_{\text{standard}} - 1 \right] \times 1000 \quad (1)$$

$$\delta^{18}\text{O} = \left[\left(\frac{^{18}\text{O}/^{16}\text{O}}{^{18}\text{O}/^{16}\text{O}} \right)_{\text{sample}} / \left(\frac{^{18}\text{O}/^{16}\text{O}}{^{18}\text{O}/^{16}\text{O}} \right)_{\text{standard}} - 1 \right] \times 1000 \quad (2)$$

Detailed information regarding the analysis procedure can be found in our previous study (Zong et al., 2017). The reduction rate of NO_3^- to NO_2^- was found to be $97.01 \pm 4.32\%$ ($n = 76$). The analytical precision determined from the replicates was less than 0.3‰ and 0.7‰ for $\delta^{15}\text{N}$ and $\delta^{18}\text{O}$, respectively, for both standards and samples. NO_2^- concentrations in $\text{PM}_{2.5}$ samples were usually lower than the detection limit and less than 1.68% of NO_3^- ; thus, they were neglected in the $\delta^{15}\text{N}$ and $\delta^{18}\text{O}$ analyses.

OC and EC were analyzed using a Desert Research Institute Model 2001 Carbon analyzer (Atmoslytic Inc., Calabasas, CA) following the Interagency Monitoring of the Protected Visual Environment thermal/optical reflectance protocol (Chow and Watson, 2002). Ionic species (SO_4^{2-} , NH_4^+ , K^+ , Ca^{2+} , Cl^- , Na^+ , Mg^{2+} , and NO_3^-) were measured using ion chromatography (Dionex ICS3000, Dionex Ltd., America) based on the reported analysis method (Feng et al., 2012). Inorganic elements (Ti, V, Cr, Mn, Fe, Co, Ni, Cu, Zn, As, Y, Cd, La, Ce, Pr, Nd, Pb, Th, U) were determined using inductively coupled plasma coupled with a mass spectrometer (ICP-MS; ELAN DRCII type, Perkin Elmer Ltd., Hong Kong) following the standard method (Tan et al., 2016). Replicate analyses showed deviations of 5.91% and 4.30% for OC and EC, respectively. The ion detection limit was 10 ng ml^{-1} with an error of <5%; the resolution of ICP-MS ranged from 0.3 to 3.0 amu with a detection limit lower than 0.01 ng ml^{-1} , and an error of <5%. We note that $\delta^{15}\text{N}$, $\delta^{18}\text{O}$, OC, EC, ions, and inorganic elements were all blank-corrected by subtracting the average field blank value.

2.3. Modelling analysis

2.3.1. Air trajectory generation

The 72 h backward trajectories with 6 hourly intervals were generated using the hybrid single-particle Lagrangian integrated trajectory (HYSPLIT) model (Zhang et al., 2014). This model is available from the National Oceanic and Atmospheric Administration Air Resource Laboratory website (www.arl.noaa.gov/ready/hysplit4.html). Trajectories were calculated for air masses starting from the sampling site at 500 m above ground level. A total of 136 trajectories were generated and then classified into three clusters using the clustering function in the HYSPLIT model.

2.3.2. Bayesian isotopic mixing model

The Bayesian isotopic mixing model can employ a stable isotopic feature to determine the probability distribution of the contribution of each source to a mixture, and explicitly account for the uncertainty associated with multiple sources, fractionation, and isotope signatures (Parnell et al., 2013). Thus, it has been widely used in scientific studies, such as food-web analyses in ecology (Moore and Semmens, 2008). However, it is challenging to apply this method in atmospheric research because it is difficult to quantify isotopic fractionation during the atmospheric transmission and transformation processes (Walters and Michalski, 2016). In our previous study, the Bayesian isotopic mixing model was improved for atmospheric research by incorporating the isotopic fractionation of the equilibrium/Leighton reaction and was adopted to apportion the annual sources of NO_x at Beihuangcheng

Island, a regional background site in China. Here, we continued to employ the improved model to identify diurnal NO_x sources at YRD. For the particular model framework and computing method, readers are referred Text S1 (Zong et al., 2017).

2.3.3. PMF model

PMF is an effective source apportionment receptor model because it does not require source profiles prior to analysis and has no limitation on source number. The principles of PMF can be found in previous study (Tao et al., 2014). In this research, PMF 5.0 was employed with the inclusion of 76 samples with 29 species (OC, EC, Cl^- , NO_3^- , SO_4^{2-} , Na^+ , NH_4^+ , K^+ , Mg^{2+} , Ca^{2+} , Ti, V, Cr, Mn, Fe, Co, Ni, Cu, Zn, As, Y, Cd, La, Ce, Pr, Nd, Pb, Th, and U) in the model computation. To confirm the optimal number of source factor, a series of tests were carried out, using 4–10 source factors (Fig. S2). The lowest Q_{Robust} value (7223) was found when seven factors were used, with an F_{Peak} value of 0, demonstrating the most physically reasonable source profile. Bootstrapping (BS), displacement (DISP), and bootstrapping with displacement (BS-DISP) near seven factors were also explored to simultaneously identify uncertainties in the PMF model (Brown et al., 2015). Using BS for six factors, three (vehicle exhaust, ship emissions, and secondary inorganic aerosol) were mapped in 100% of the runs, while coal combustion, soil dust, and industry emissions were mapped in 82%, 81%, and 93% of the runs, respectively. There were no swaps with DISP, and 98% of the BS-DISP runs were successful. For seven factors, results were more stable; all factors, with the exception of sea salt (mapped in 94% of runs), were always mapped in BS (Table S2), no swaps occurred with DISP and all BS-DISP runs were successful. When eight factors were evaluated, the solution became unstable. The added Cr industry factor was mapped in 72% of runs, sea salt was mapped 90% of the time, and other factors were always mapped. No swaps were found in DISP; however, 28% of BS-DISP runs were rejected due to factor swaps. Consequently, results suggest that seven source factors were optimal in this study.

3. Results and discussion

3.1. Source signals and factors affecting NO_x conversion

NO_3^- concentrations were distributed over a wide range ($2.28\text{--}48.64 \mu\text{g m}^{-3}$), with an average of $14.43 \mu\text{g m}^{-3}$. It was the second most abundant component ($15.36 \pm 4.70\%$) in $\text{PM}_{2.5}$, following SO_4^{2-} ($22.12 \pm 6.25\%$). Comparatively, NO_3^- concentrations were higher than the observations reported in other regions of China during summer, including both urban areas (e.g., Lanzhou, Linan) and background sites (e.g., Tuoji Island) (Wang et al., 2014, 2016; Zhang et al., 2017a). This implies that NO_3^- pollution was relatively severe in YRD during our analysis. To explore the formation mechanisms of NO_3^- , its relationship with meteorological parameters is analyzed as shown in Fig. S3. Wind speed and relative humidity do not significantly impact NO_3^- concentration and, while the influence of temperature is comparatively greater, its impact on NO_3^- variation is still weak. However, the correlation of the first order difference in NO_3^- concentration and meteorological parameters exhibits an obvious rise, suggesting that high-frequency variations in meteorological parameters may be closely linked with the generation of NO_3^- . This finding may explain the tendency for severe pollution episodes with high NO_3^- concentrations to accompany unsettled weather in North China (Xue et al., 2016).

The average daytime concentration of NO_3^- ($16.96 \pm 8.67 \mu\text{g m}^{-3}$) was higher as compared to the night time ($12.04 \pm 7.27 \mu\text{g m}^{-3}$) concentration. A homothetic phenomenon was apparent for the $\text{NO}_3^-/\text{PM}_{2.5}$ ratio, with mean values of $16.49 \pm 4.68\%$ and $14.23 \pm 4.57\%$ during the day and night, respectively. Higher daytime

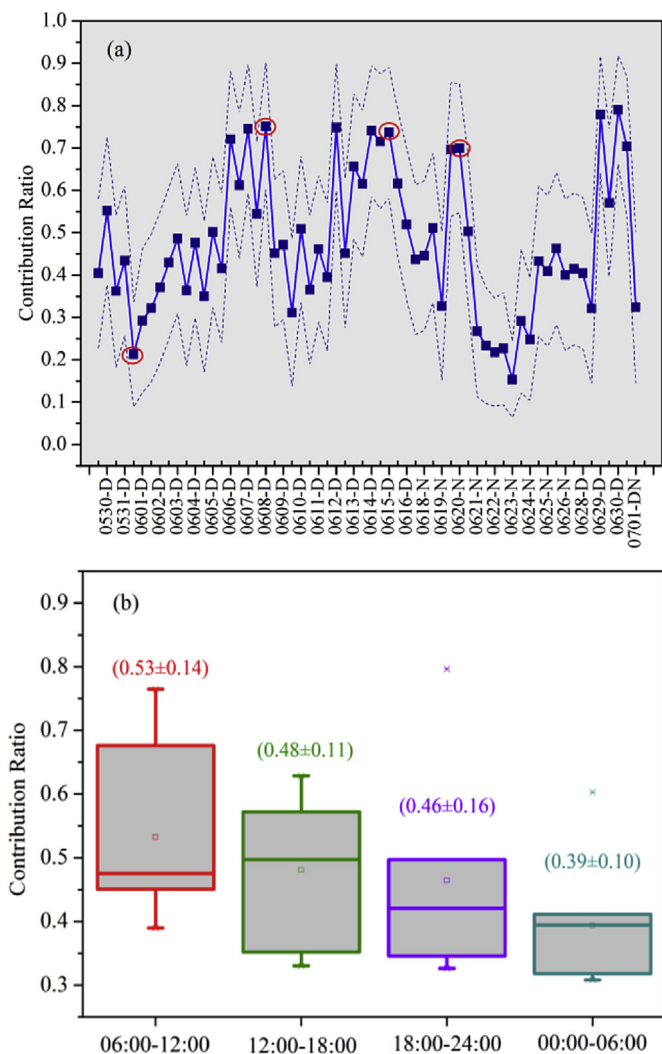


Fig. 2. (a) Range (dotted line) and median (solid line) of contribution ratio of •OH generation pathway indicated by Bayesian mixing model during the sampling period. "D" is the day time and "N" refers to the night time in the sampling period; (b) sub-divided contribution ratio in 6-h scale.

burning ($+1.04 \pm 4.13\%$), and microbial processes ($-33.77 \pm 12.16\%$) were considered to be the dominant sources of NO_x at YRD (Text S4; Table S3; Fig. S7). The improved Bayesian isotopic mixing model was run for three patterns, the overall simulation, diurnal simulation, and clustering simulation, to investigate NO_x sources. The overall simulation shows that coal combustion was the most significant source of NO_x ($31.34 \pm 9.04\%$), followed by biomass burning ($25.74 \pm 2.58\%$), mobile sources ($23.83 \pm 3.66\%$), and microbial processes ($19.09 \pm 5.21\%$; Fig. 3). This finding is consistent with the summer observations at Beihuangcheng Island, implying that emission sources in North China display a regional character. Coal combustion (e.g., power plants) remains the primary source of NO_x , although the widespread use of depollution devices, such as selective catalytic reduction or selective noncatalytic reduction systems, have greatly reduced the emission load from coal combustion in China (Zhao et al., 2013). As reported by the National Energy Administration, the amount of thermal power generation in the Shandong and Jiangsu Provinces have ranked first and second, respectively, in China by 2017 (<http://www.nea.gov.cn/>). Thus, backward trajectories, which generally pass through these two provinces (Fig. S1), provide further

evidence to support coal combustion as the most significant source of NO_x at YRD (see also the contribution of coal combustion in cluster 2 in Fig. S5). Biomass burning (e.g., forest clearing for agricultural use, cooking, and heating) has been neglected as a potential NO_x source in previous studies. However, in recent years, the prevalence of large-scale biomass burning and household emissions without any pollution control mechanisms has markedly increased emissions from this source. For example, NO_x emissions from biomass burning increased more than six-fold between 1990 and 2013 in China (Li et al., 2016).

With the rapid growth in car ownership in China, vehicle exhaust has become an increasing source of NO_x , which has been verified by the recent emission inventory (Lu et al., 2016). Furthermore, it was found that 11.30% of NO_x in China could be attributed to ship emissions, with coastal regions being the most affected areas (Zhang et al., 2016). Hence, NO_x from mobile sources could be also attributed to ship emissions in the Bohai region. YRD is a representative coastal wetland system in North China, serving as an important example of land and ocean interactions. Thus, the biogeochemical processes in the region may control the quantity and distribution of NO_x (Yu et al., 2016), especially during instances of hot and rainy weather during summer. Moreover, as a consequence of agricultural lands and ocean surroundings, emissions from integrated microbial processes (e.g., biogenic soil and ocean processes) are a NO_x source at YRD.

Fig. 3 displays the diurnal variation of the four NO_x sources. Contributions did not show any significant diurnal variation ($p > 0.05$); however, differences were still apparent. For example, coal combustion and biomass burning contributed more during night time, consistent with the correlation coefficients between coal combustion tracers and NO_3^- (Fig. 1). A reasonable explanation for this phenomenon is that nearby power plants often emit more pollutant overnight to avoid inspection after a serious haze pollution incident in January 2013 in North China. Moreover, during the sampling period, sunset occurred at approximately 20:00. Hence, a portion of night time sampling (18:00–20:00 p.m.) occurred when the environment was conducive for farmers to cook or burn biomass (e.g., open burning and household exhaust). Conversely, emissions from mobile sources and microbial processes peaked during daytime, which coincides with traffic and shipping rush hours. Furthermore, high emissions from microbial processes occur during the day due to high temperatures and ample sunlight (Wang et al., 2007). The clustering contributions from the four sources are summarized in Fig. S5. It is apparent that the contributions from biomass burning and coal combustion were higher in cluster 2, when backward trajectories were from the Shandong and Jiangsu Provinces due to high amounts of thermal power generation. Furthermore, previous study has shown that biomass burning in these two provinces was an important source of pollutants at YRD during summer (Zong et al., 2015). Comparatively, a slight increase in the contributions from mobile sources and microbial processes in cluster 3 correspond to ship emissions and microbial processes from the ocean region. There was no notably high value for any of the four sources in cluster 1, indicating relatively mixed NO_x sources from the Hebei Province.

3.4. Source apportionment of NO_3^- using the PMF model

EPA PMF5.0 model was used together with a data set of 76×29 (76 samples with 29 species) to further apportion the sources of NO_3^- in YRD. Based on the results of the PMF model, seven factors were identified; sea salt, vehicle exhaust, ship emissions, coal combustion, soil dust, secondary inorganic aerosol and industry emissions. Simulated source profiles and the relative contribution of individual sources to each species are displayed in Fig. 4. The first

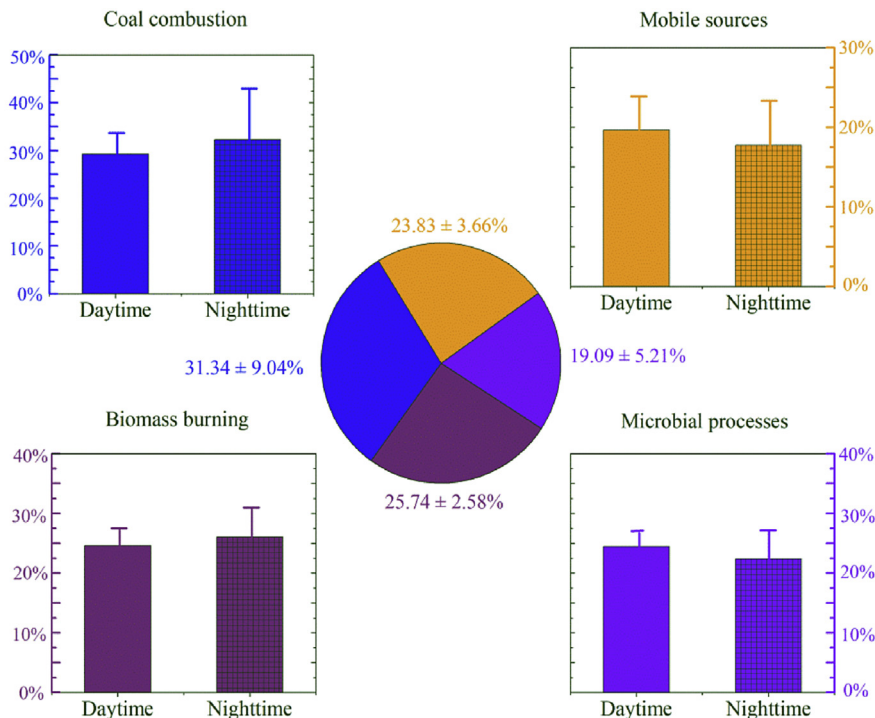


Fig. 3. Total and diurnal contributions of coal combustion, mobile sources, biomass burning and microbial processes to NO_x at YRD.

factor, sea salt, is characterized by high contributions of Na⁺ and Mg²⁺, which are related to the primary sea salt aerosol produced by mechanical disruption of the ocean surface (Zong et al., 2016). The Cl⁻/Na⁺ was 1.31 in this factor, lower than the average ratio in seawater (1.80). This may be related to Cl⁻ depletion during transportation, especially during summer (Masiol et al., 2017). The second factor, vehicle exhaust, displays high loadings of EC, Cu, Zn, Cd, and NH₄⁺. Following the growth of car ownership, vehicles equipped with three-way catalytic converters are an important source of NH₄⁺ (Liu et al., 2014b). Furthermore, EC, Zn, Cu, and Cd are usually emitted as bound particles from vehicle exhaust. The third factor contributes high proportions of V and Ni, which are associated with emissions from residual oil and are suggestive of ship emissions. A V/Ni ratio >0.70 is widely considered to be a sign of particles influenced by ship emissions. In this factor, the V/Ni ratio was 1.41, which similar with that of Tuoji Island, a region considered to be influenced by ship emissions (Zhang et al., 2014). The fourth source, coal combustion, is characterized by high contributions of EC, Cl⁻, SO₄²⁻, As, and Pb. Coal combustion is often indicated by elevated Cl⁻ linked with high EC and SO₄²⁻ (Zhang et al., 2013). Utilizing the depleted Cl⁻/Na⁺ value in the first factor, the contribution of non-sea-salt emissions for Cl⁻ was 60.50%, consistent with the portion in this factor. Since 2000, leaded gasoline has been banned in China, leading to coal combustion being the primary source of Pb. Moreover, a high As loading is frequently used as an indicator of emissions from coal-fired power stations (Tao et al., 2014).

The fifth factor is classified as soil dust with some typical crustal components, including Ca²⁺, Ti, Mn, Fe, and rare earth elements. Generally, Ca, Ti, and Fe are deemed to be the major constituents for soil dust and have been adopted as the reference elements in the enrichment factor calculation (Tan et al., 2014), similar to the analysis in this study. The sixth factor, secondary inorganic aerosol, is characterized by high contributions of NO₃⁻, SO₄²⁻, and NH₄⁺. These secondary aerosols are mainly derived from the conversions

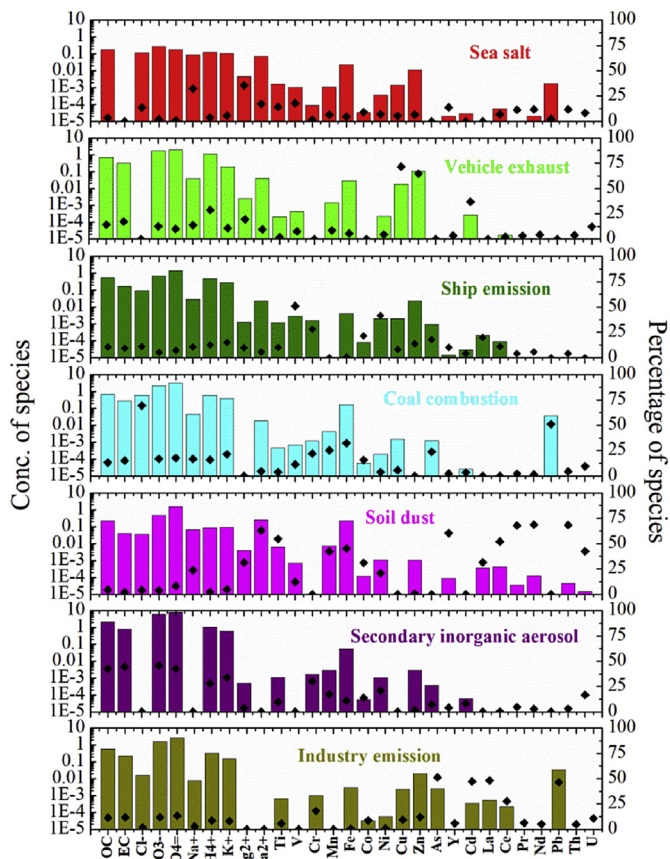


Fig. 4. Source profiles (bars; unit: μg m⁻³) and contribution percentage (dots; unit: %) of the seven factors resolved from PMF model.

of their precursor gases, including NO_x , SO_2 , and NH_3 emissions from vehicle exhaust, coal combustion and biomass burning. Because vehicle exhaust and coal combustion have been classified individually, biomass burning is likely to be the source for this factor. This is further indicated by the high contributions of OC, EC, and K^+ in this instance. K^+ is an excellent tracer for biomass burning (Wang et al., 2017a), and our previous research confirmed that biomass burning was an important source for OC and EC at YRD based on radiocarbon analysis (Zong et al., 2015). The final source factor is classified as typical industry emissions, presenting high percentages of Cr, Cd, As, Pb, and so on. The proportions of Pb and As in this factor parallel those of coal combustion, indicating that industry emissions originate from coal burning in industrial processes.

The contributions of these seven factors to NO_3^- are summarized in Fig. S6. Secondary inorganic aerosol, coal combustion, and vehicle exhaust were the main contributors, accounting for 45.60%, 16.90%, and 12.70%, respectively. They were followed by industry emissions (11.75%), ship emissions (7.13%), soil dust (3.81%), and sea salt (2.11%). To verify this estimation, results were compared with those from a Bayesian isotopic mixing model (Fig. 5). For better comparison, vehicle exhaust and ship emissions in the PMF model were classified together as mobile sources because of their similar characteristics. Furthermore, industry emissions were classified with coal combustion due to their origins from coal burning. Accordingly, mobile sources in the PMF simulation sum to 19.83%, slightly lower than the Bayesian value (23.83%). A similar pattern was found for coal combustion (28.65% in the PMF simulation as compared to 31.34% in the Bayesian model). We note that biomass burning and microbial processes were not identified in the PMF model; however, secondary inorganic aerosol, sea salt, and soil dust were represented. As previously discussed, biomass burning is likely to be the primary source of secondary inorganic aerosol. NO_3^- from microbial processes including biogenic soil and ocean processes are mainly secondary products. Thus, we compare the sum of biomass burning and microbial processes in the Bayesian result (44.83%) with the aggregate of secondary inorganic aerosol, sea salt, and soil dust in PMF (51.52%). Differences between the two models were relatively minor, with the largest discrepancy of 6.69%, being mainly attributed to irrelevant classifications. For example, NO_3^- from soil dust may derive from re-suspension, which could in fact represent primary materials. Overall, the two models generally agreed, suggesting that our study provides a reasonable source apportionment of $\text{NO}_x \sim \text{NO}_3^-$ at YRD during summer.

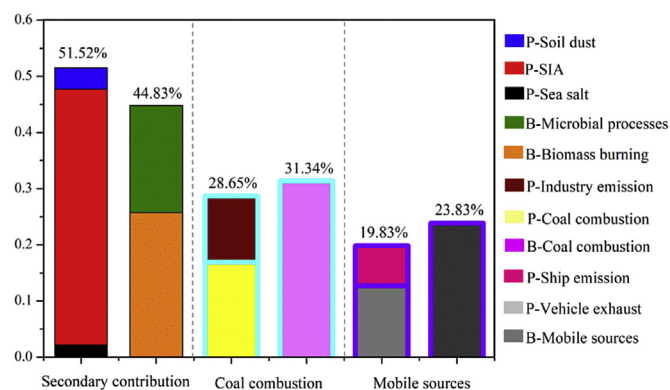


Fig. 5. Comparison of source apportionment results of NO_x between Bayesian mixing model and PMF model, “P” represents the PMF result including P-SIA, P-Sea salt, P-Industry emission, P-Coal combustion, P-Ship emission, P-Vehicle exhaust; “B” refers to the Bayesian mixing model result consisting of B-Microbial processes, B-Biomass burning, B-Coal combustion and B-Mobile sources.

4. Conclusion

Our results showed that the observed concentrations of NO_3^- were relatively high as compared to previous research, implying severe NO_3^- pollution during the study period at YRD. Based on the correlation analysis with tracer species, NO_3^- was found to originate from typical combustion sources with an apparent diurnal variation. $\delta^{15}\text{N}-\text{NO}_3^-$ varied between -8.9‰ and $+14.1\text{‰}$, and $\delta^{18}\text{O}-\text{NO}_3^-$ ranged from $+57.4\text{‰}$ to $+93.8\text{‰}$. Using an improved Bayesian isotopic mixing model, the median proportion of the $\bullet\text{OH}$ generation pathway had a clear diurnal fluctuation which was higher during the day (0.53 ± 0.16) and lower overnight (0.42 ± 0.17). At a 6 hourly timescale, the $\bullet\text{OH}$ generation pathway decreased gradually from 06:00–12:00 to 24:00–06:00 with maximum of 0.53 and a minimum of 0.39, respectively.

Coal combustion ($31.34 \pm 9.04\%$) was the dominant emission source, followed by biomass burning ($25.74 \pm 2.58\%$), mobile sources ($23.83 \pm 3.66\%$), and microbial processes ($19.09 \pm 5.21\%$). Diurnally, NO_x from coal combustion and biomass burning was higher at night, while NO_x from mobile sources and microbial processes peaked during the daytime. Seven factors; sea salt, vehicle exhaust, ship emissions, coal combustion, soil dust, secondary inorganic aerosol, and industry emissions were identified based on the PMF simulation. Among these factors, secondary inorganic aerosol, coal combustion, and vehicle exhaust were the major contributors, accounting for 45.60%, 16.90%, and 12.70%, respectively. Industry emissions (11.75%), ship emissions (7.13%), soil dust (3.81%), and sea salt (2.11%) contributed less to emissions. Comparatively, mobile sources in the PMF simulation contributed 19.83%, slightly lower as compared to the Bayesian value (23.83%). Coal combustion followed the same pattern, with a contribution of 28.65% according to PMF results and 31.34% in the Bayesian model. The sum of biomass burning and microbial processes in the Bayesian model (44.83%) was lower than the aggregate of secondary inorganic aerosol, sea salt, and soil dust in the PMF model (51.52%). In summary, differences between the two models were minor, indicating that our estimation provided a reasonable source apportionment for $\text{NO}_x \sim \text{NO}_3^-$ at YRD during summer. The findings will help to improve air quality in the seriously polluted region of North China.

Notes

The authors declare no competing financial interest.

Acknowledgment

This work was financially supported by Project funded by China Postdoctoral Science Foundation (2017M622815), Key Laboratory of Coastal Environmental Processes and Ecological Remediation of the Chinese Academy of Sciences (CAS) (Grant No: 2016KFJJ01), the National Scientific Foundation of China (NSFC; Grant Nos: 41471413 and 31370464). The authors gratefully acknowledge the National Oceanic and Atmospheric Administration’s Air Resources Laboratory for providing the HYSPLIT transport model and the READY website (<http://www.arl.noaa.gov/ready.html>). All data in this study are freely available on request through the corresponding author (cgtian@yic.ac.cn).

Appendix A. Supplementary data

Supplementary data related to this article can be found at <https://doi.org/10.1016/j.envpol.2018.08.026>.

References

- Beyn, F., Matthias, V., Aulinger, A., Daehnke, K., 2015. Do N-isotopes in atmospheric nitrate deposition reflect air pollution levels? *Atmos. Environ.* 107, 281–288.
- Bressi, M., Sciare, J., Gherzi, V., Mihalopoulos, N., Petit, J.E., Nicolas, J.B., et al., 2014. Sources and geographical origins of fine aerosols in Paris (France). *Atmos. Chem. Phys.* 14, 8813–8839.
- Brown, S.G., Eberly, S., Paatero, P., Norris, G.A., 2015. Methods for estimating uncertainty in PMF solutions: examples with ambient air and water quality data and guidance on reporting PMF results. *Sci. Total Environ.* 518–519, 626–635.
- Chen, D., Wang, X., Li, Y., Lang, J., Zhou, Y., Guo, X., et al., 2017. High-spatiotemporal-resolution ship emission inventory of China based on AIS data in 2014. *Sci. Total Environ.* 609, 776–787.
- Chen, W., Tang, H., Zhao, H., 2015. Diurnal, weekly and monthly spatial variations of air pollutants and air quality of Beijing. *Atmos. Environ.* 119, 21–34.
- Cheng, Y., Zheng, G., Wei, C., Mu, Q., Zheng, B., Wang, Z., et al., 2016. Reactive nitrogen chemistry in aerosol water as a source of sulfate during haze events in China. *Sci. Adv.* 2, e1601530.
- Chow, J.C., Watson, J.G., 2002. PM_{2.5} carbonate concentrations at regionally representative Interagency Monitoring of Protected Visual Environment sites. *J. Geophys. Res. Atmos.* 107, 8344.
- Elliott, E.M., Kendall, C., Wankel, S.D., Burns, D.A., Boyer, E.W., Harlin, K., et al., 2007. Nitrogen isotopes as indicators of NO_x source contributions to atmospheric nitrate deposition across the Midwestern and northeastern United States. *Environ. Sci. Technol.* 41, 7661–7667.
- Fang, Y., Chen, Y., Tian, C., Lin, T., Hu, L., Li, J., et al., 2016. Application of PMF receptor model merging with PAHs signatures for source apportionment of black carbon in the continental shelf surface sediments of the Bohai and Yellow Seas, China. *J. Geophys. Res. Oceans* 121, 1346–1359.
- Fang, Y.T., Koba, K., Wang, X.M., Wen, D.Z., Li, J., Takebayashi, Y., et al., 2011. Anthropogenic imprints on nitrogen and oxygen isotopic composition of precipitation nitrate in a nitrogen-polluted city in southern China. *Atmos. Chem. Phys.* 11, 1313–1325.
- Feng, J.L., Guo, Z.G., Zhang, T.R., Yao, X.H., Chan, C.K., Fang, M., 2012. Source and formation of secondary particulate matter in PM_{2.5} in Asian continental outflow. *J. Geophys. Res.: Atmosphere* 117, D03302.
- Fibiger, D.L., Hastings, M.G., 2016. First measurements of the nitrogen isotopic composition of NO_x from biomass burning. *Environ. Sci. Technol.* 50, 11569–11574.
- Han, G., Chu, X., Xing, Q., Li, D., Yu, J., Luo, Y., et al., 2015. Effects of episodic flooding on the net ecosystem CO₂ exchange of a supratidal wetland in the Yellow River Delta. *J. Geophys. Res. Biogeosci.* 120, 1506–1520.
- Hastings, M.G., Jarvis, J.C., Steig, E.J., 2009. Anthropogenic impacts on nitrogen isotopes of ice-core nitrate. *Science* 324, 1288–1288.
- Hastings, M.G., Sigman, D.M., Lipschultz, F., 2003. Isotopic evidence for source changes of nitrate in rain at Bermuda. *J. Geophys. Res.: Atmosphere* 108, 4790.
- Hastings, M.G., Steig, E.J., Sigman, D.M., 2004. Seasonal variations in N and O isotopes of nitrate in snow at Summit, Greenland: implications for the study of nitrate in snow and ice cores. *J. Geophys. Res. Atmos.* 109, D20306.
- Huang, R.-J., Zhang, Y., Bozzetti, C., Ho, K.-F., Cao, J.-J., Han, Y., et al., 2014. High secondary aerosol contribution to particulate pollution during haze events in China. *Nature* 514, 218–222.
- Li, J., Li, Y., Bo, Y., Xie, S., 2016. High-resolution historical emission inventories of crop residue burning in fields in China for the period 1990–2013. *Atmos. Environ.* 138, 152–161.
- Liu, J.W., Li, J., Zhang, Y.L., Liu, D., Ding, P., Shen, C.D., et al., 2014a. Source apportionment using radiocarbon and organic tracers for PM_{2.5} carbonaceous aerosols in Guangzhou, south China: contrasting local- and regional-scale haze events. *Environ. Sci. Technol.* 48, 12002–12011.
- Liu, T., Wang, X., Wang, B., Ding, X., Deng, W., Lu, S., et al., 2014b. Emission factor of ammonia (NH₃) from on-road vehicles in China: tunnel tests in urban Guangzhou. *Environ. Res. Lett.* 9, 064027.
- Liu, X., Zhang, Y., Han, W., Tang, A., Shen, J., Cui, Z., et al., 2013. Enhanced nitrogen deposition over China. *Nature* 494, 459–462.
- Lu, X., Yao, T., Li, Y., Fung, J.C., Lau, A.K., 2016. Source apportionment and health effect of NO_x over the Pearl River Delta region in southern China. *Environ. Pollut.* 212, 135–146.
- Masiol, M., Hopke, P.K., Felton, H.D., Frank, B.P., Rattigan, O.V., Wurth, M.J., et al., 2017. Source apportionment of PM_{2.5} chemically speciated mass and particle number concentrations in New York City. *Atmos. Environ.* 148, 215–229.
- McIlvin, M.R., Altabet, M.A., 2005. Chemical conversion of nitrate and nitrite to nitrous oxide for nitrogen and oxygen isotopic analysis in freshwater and seawater. *Anal. Chem.* 77, 5589–5595.
- Miller, D.J., Wojtal, P.K., Clark, S.C., Hastings, M.G., 2017. Vehicle NO_x emission plume isotopic signatures: spatial variability across the eastern United States. *J. Geophys. Res. Atmos.* 122, 4698–4717.
- Moore, J.W., Semmens, B.X., 2008. Incorporating uncertainty and prior information into stable isotope mixing models. *Ecol. Lett.* 11, 470–480.
- Morin, S., Savarino, J., Frey, M.M., Domine, F., Jacobi, H.W., Kaleschke, L., et al., 2009. Comprehensive isotopic composition of atmospheric nitrate in the Atlantic Ocean boundary layer from 65 degrees S to 79 degrees N. *J. Geophys. Res. Atmos.* 114, D05303.
- Parnell, A.C., Phillips, D.L., Bearhop, S., Semmens, B.X., Ward, E.J., Moore, J.W., et al., 2013. Bayesian stable isotope mixing models. *Environmetrics* 24, 387–399.
- Tan, J., Duan, J., Ma, Y., He, K., Cheng, Y., Deng, S.X., et al., 2016. Long-term trends of chemical characteristics and sources of fine particle in Foshan City, Pearl River Delta: 2008–2014. *Sci. Total Environ.* 565, 519–528.
- Tan, J.H., Duan, J.C., Ma, Y.L., Yang, F.M., Cheng, Y., He, K.B., et al., 2014. Source of atmospheric heavy metals in winter in Foshan, China. *Sci. Total Environ.* 493, 262–270.
- Tao, J., Gao, J., Zhang, L., Zhang, R., Che, H., Zhang, Z., et al., 2014. PM_{2.5} pollution in a megacity of southwest China: source apportionment and implication. *Atmos. Chem. Phys.* 14, 8679–8699.
- Walters, W.W., Goodwin, S.R., Michalski, G., 2015a. Nitrogen stable isotope composition ($\delta^{15}\text{N}$) of vehicle-emitted NO_x. *Environ. Sci. Technol.* 49, 2278–2285.
- Walters, W.W., Michalski, G., 2016. Theoretical calculation of oxygen equilibrium isotope fractionation factors involving various NO_y molecules, OH, and H₂O and its implications for isotope variations in atmospheric nitrate. *Geochim. Cosmochim. Acta* 191, 89–101.
- Walters, W.W., Sharp, B.D., Fang, H., Kozak, B.J., Michalski, G., 2015b. Nitrogen isotope composition of thermally produced NO_x from various fossil-fuel combustion sources. *Environ. Sci. Technol.* 49, 11363–11371.
- Wang, X., Chen, Y., Tian, C., Huang, G., Fang, Y., Zhang, F., et al., 2014. Impact of agricultural waste burning in the Shandong Peninsula on carbonaceous aerosols in the Bohai Rim, China. *Sci. Total Environ.* 481, 311–316.
- Wang, X., Zong, Z., Tian, C., Chen, Y., Luo, C., Li, J., et al., 2017a. Combining positive matrix factorization and radiocarbon measurements for source apportionment of PM_{2.5} from a national background site in North China. *Scientific Rep.* 7, 10648.
- Wang, Y.-L., Liu, X.-Y., Song, W., Yang, W., Han, B., Dou, X.-Y., et al., 2017b. Source apportionment of nitrogen in PM_{2.5} based on bulk $\delta^{15}\text{N}$ signatures and a Bayesian isotope mixing model. *Tellus B* 69, 1299672.
- Wang, Y., Jia, C., Tao, J., Zhang, L., Liang, X., Ma, J., et al., 2016. Chemical characterization and source apportionment of PM_{2.5} in a semi-arid and petrochemical-industrialized city, Northwest China. *Sci. Total Environ.* 573, 1031–1040.
- Wang, Y., McElroy, M.B., Martin, R.V., Streets, D.G., Zhang, Q., Fu, T.-M., 2007. Seasonal variability of NO_x emissions over east China constrained by satellite observations: implications for combustion and microbial sources. *J. Geophys. Res. Atmos.* 112, D06301.
- Wankel, S.D., Chen, Y., Kendall, C., Post, A.F., Paytan, A., 2010. Sources of aerosol nitrate to the Gulf of Aqaba: evidence from $\delta^{15}\text{N}$ and $\delta^{18}\text{O}$ of nitrate and trace metal chemistry. *Mar. Chem.* 120, 90–99.
- Xiao, H.-W., Xie, L.-H., Long, A.-M., Ye, F., Pan, Y.-P., Li, D.-N., et al., 2015. Use of isotopic compositions of nitrate in TSP to identify sources and chemistry in South China Sea. *Atmos. Environ.* 109, 70–78.
- Xue, J., Yuan, Z., Griffith, S.M., Yu, X., Lau, A.K., Yu, J.Z., 2016. Sulfate formation enhanced by a cocktail of high NO_x, SO₂, particulate matter, and droplet pH during haze-fog events in megacities in China: an observation-based modeling investigation. *Environ. Sci. Technol.* 50, 7325–7334.
- Yang, Y.R., Liu, X.G., Qu, Y., An, J.L., Jiang, R., Zhang, Y.H., et al., 2015. Characteristics and formation mechanism of continuous hazes in China: a case study during the autumn of 2014 in the North China Plain. *Atmos. Chem. Phys.* 15, 8165–8178.
- Yu, J., Zhan, C., Li, Y., Zhou, D., Fu, Y., Chu, X., et al., 2016. Distribution of carbon, nitrogen and phosphorus in coastal wetland soil related land use in the Modern Yellow River Delta. *Scientific Rep.* 6, 37940.
- Zhang, F., Chen, Y., Tian, C., Lou, D., Li, J., Zhang, G., et al., 2016. Emission factors for gaseous and particulate pollutants from offshore diesel engine vessels in China. *Atmos. Chem. Phys.* 16, 6319–6334.
- Zhang, F., Chen, Y., Tian, C., Wang, X., Huang, G., Fang, Y., et al., 2014. Identification and quantification of shipping emissions in Bohai Rim, China. *Sci. Total Environ.* 497–498, 570–577.
- Zhang, R., Jing, J., Tao, J., Hsu, S.C., Wang, G., Cao, J., et al., 2013. Chemical characterization and source apportionment of PM_{2.5} in Beijing: seasonal perspective. *Atmos. Chem. Phys.* 13, 7053–7074.
- Zhang, Y., Zhang, H., Deng, J., Du, W., Hong, Y., Xu, L., et al., 2017a. Source regions and transport pathways of PM_{2.5} at a regional background site in East China. *Atmos. Environ.* 167, 202–211.
- Zhang, Z., Gao, J., Zhang, L., Wang, H., Tao, J., Qiu, X., et al., 2017b. Observations of biomass burning tracers in PM_{2.5} at two megacities in North China during 2014 APEC summit. *Atmos. Environ.* 169, 54–64.
- Zhao, B., Wang, S., Wang, J., Fu, J.S., Liu, T., Xu, J., et al., 2013. Impact of national NO_x and SO₂ control policies on particulate matter pollution in China. *Atmos. Environ.* 77, 453–463.
- Zong, Z., Chen, Y., Tian, C., Fang, Y., Wang, X., Huang, G., et al., 2015. Radiocarbon-based impact assessment of open biomass burning on regional carbonaceous aerosols in North China. *Sci. Total Environ.* 518–519, 1–7.
- Zong, Z., Wang, X., Tian, C., Chen, Y., Fang, Y., Zhang, F., et al., 2017. First assessment of NO_x sources at a regional background site in North China using isotopic analysis linked with modeling. *Environ. Sci. Technol.* 51, 5923–5931.
- Zong, Z., Wang, X., Tian, C., Chen, Y., Qu, L., Ji, L., et al., 2016. Source apportionment of PM_{2.5} at a regional background site in North China using PMF linked with radiocarbon analysis: insight into the contribution of biomass burning. *Atmos. Chem. Phys.* 16, 11249–11265.